Stator Winding Fault Diagnosis of Permanent Magnet Synchronous Motor-Based DTC–SVM Dedicated to Electric Vehicle

1 author:

Fatma Ben Salem
University of Sfax
45 PUBLICATIONS   **325** CITATIONS

We are IntechOpen,
the world's leading publisher of
Open Access books
Built by scientists, for scientists

5,000
Open access books available

124,000
International authors and editors

140M
Downloads

Our authors are among the

154
Countries delivered to

TOP 1%
most cited scientists

12.2%
Contributors from top 500 universities

CLARIVATE ANALYTICS
BOOK CITATION INDEX
INDEXED

WEB OF SCIENCE™

Selection of our books indexed in the Book Citation Index
in Web of Science™ Core Collection (BKCI)

Interested in publishing with us?
Contact book.department@intechopen.com

Numbers displayed above are based on latest data collected.
For more information visit www.intechopen.com

Stator Winding Fault Diagnosis of Permanent Magnet Synchronous Motor-Based DTC-SVM Dedicated to Electric Vehicle Applications

Fatma Ben Salem

Abstract

Electric vehicles (EVs) have several advantages such as energy efficiency, virtually lack of pollution, and the availability of electric energy through electric distribution systems. Among the major components of an EV is the block control of the AC motor. Many modern high-performance control technologies are being used in EV controllers, such as direct torque control-based space vector modulation (DTC-SVM). Given that permanent magnet synchronous motor (PMSM) has a small volume, a lightweight, and a high reliability, attracting the interest of EV industrial designers. The fault diagnosis about the PMSM problems is essential because the PMSM has a huge influence on the safety and economic efficiency with the vehicles. In this background, the chapter concerns the modeling and simulation of an electric vehicle drive system including a PMSM-based DTC-SVM without and with stator winding fault. The performance of the motor under both the normal and faulty conditions is simulated. For the diagnosis of the fault, the chapter proposes the technique based on the motor current spectrum analysis.

Keywords: permanent magnet synchronous motor, electric vehicles, DTC-SVM, stator winding fault, diagnosis, fault signature extraction

1. Introduction

Electric vehicles (EVs) have several advantages such as energy efficiency, virtually lack of pollution, and the availability of electric energy through electric distribution systems [1–4]. Among the major components of an electric vehicle is the controlling block of the AC motor. The controller should be designed to make the drive system robust and efficient on both dynamic and steady-state performances.

Many modern high-performance control technologies are being used in EV controllers, such as direct torque control-based space vector modulation (DTC-SVM) [5–12]. The advantage of the DTC-SVM methodology is that it has all the merits of DTC strategy [13–16] by adding the fact of having a fixed switching frequency, which guarantees low vibrations in order to provide passenger comfort.

Permanent magnet synchronous motor (PMSM) becomes more suitable in wide speed range application due to their high efficiency and wide constant power speed range. In fact, the absence of rotor windings and therefore the absence of external

excitation increase the efficiency of the PMSM and greatly reduce its maintenance cost. In addition, the drop in the price of permanent magnets promotes a strong use of this type of machine particularly in the field of electric vehicle applications [17–20]. In fact, such motor has a small volume, lightweight, and high reliability attracting the interest of EV industrial designers.

So the fault diagnosis about the PMSM problems is essential because the PMSM has a huge influence on the safety and economic efficiency of the vehicles. The stator winding fault is a common fault that has interested researchers for many years [21–27]. It is resulting from the degradation of the inter-turn interphase and main isolation of the motor winding. This internal fault will increase the torque ripples that deteriorate machine performance. However such fault can be rapidly propagated to motor stator turn since it makes a large circulating current in the shorted path yielding excessive heat. The adverse condition of heat will occasionally lead to the progressive deterioration and eventual breakdown of winding insulation in the phase of the motor.

Several methods have been used to detect and estimate the type and the degree of this fault in PMSM. The motor signature current analysis is one of the most common online methods for fault detection. In fact, it is widely used in the field of PMSM fault diagnosis, because it is fast and does not need any specific model. This method uses spectral analysis techniques by comparing the healthy to the faulty case; faults can be detected.

In this chapter, as for signal processing tools, fast Fourier transform (FFT) is used to extract the frequency characteristics of the stator current signal. This method will be proposed to detect whether a PMSM, under DTC-SVM traction system, is healthy or faulty.

The chapter is organized as follows. Electric vehicle propulsion system scheme is developed in Section 2. In Section 3, the mathematical model of PMSM in (a, b, c) frame in healthy conditions is introduced and which is followed by Section 4, the PMSM with inter-turn fault modeling. Then, the design of a conventional DTC-SVM traction system is presented. Simulation result, considering steady-state operation, is discussed in Section 6.

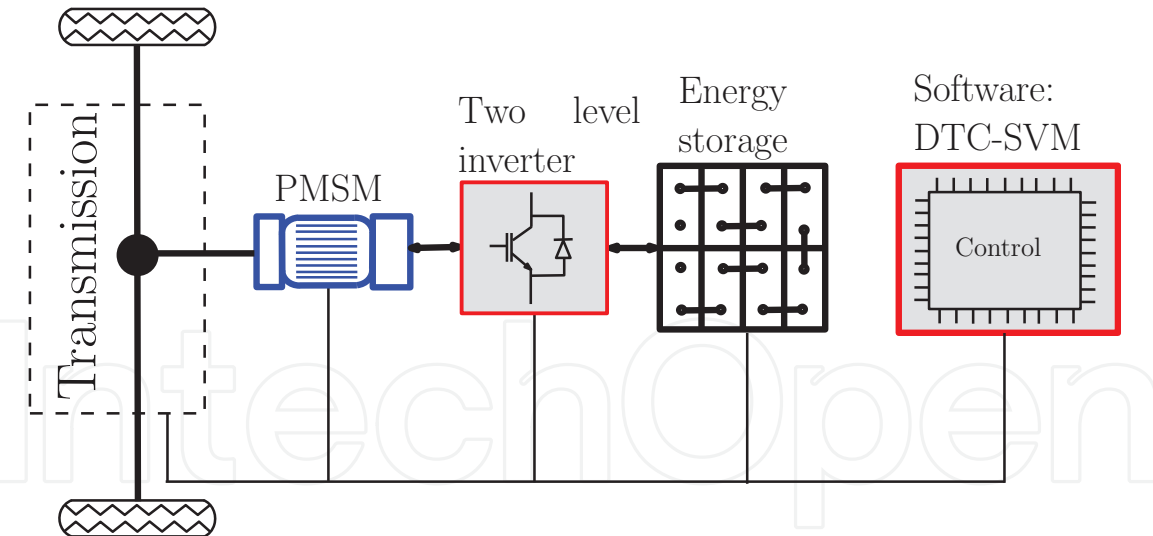## 2. Electric vehicle propulsion system scheme

The major electric propulsion system of EV consists of motor, controller, power source, charger, transmission device, and wheels (**Figure 1**) [28]. The proposed motor drive includes the electric motor (PMSM), power converter (three-phase voltage inverter), energy storage (battery), and electronic controller (DTC-SVM). These components are the core of the EV propulsion system.

The tractive effort (F_{te}) is the force propelling the vehicle forward, transmitted to the ground through the drive wheels. Consider a vehicle of mass M_v, proceeding at a velocity V_v, as in **Figure 2**. The force propelling the vehicle forward, the tractive effort, has to overcome the following forces:
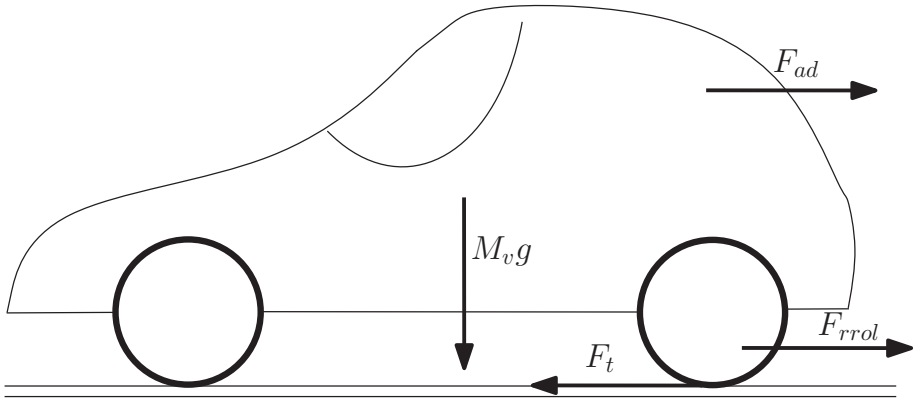
- The rolling resistance force: $F_{rrol} = \mu M_v g$

where μ is the coefficient of rolling resistance ($\mu = 0.005$ for tires developed especially for electric vehicles), M_v is the vehicle mass, and g is the gravitational constant

- The aerodynamic drag: $F_{ad} = \frac{1}{2}\rho A C_d V_v^2$

Figure 1.
Components of electric vehicle propulsion system.

Figure 2.
The forces acting on a vehicle.

where ρ is the air density, A is the frontal area, C_d is the drag coefficient, and V_v is the vehicle speed

• The hill climbing force: $F_{hc} = M_v g \sin \alpha$

where α is the angle of a slope for a vehicle climbing a hill (in the case of **Figure 2** $\alpha = 0$).

F_{te} is equal to the sum of the resistance forces [28, 29], as shown in the sequel equation:

$$F_{te} = F_{rrol} + F_{ad} + F_{hc} \tag{1}$$

2.1 Voltage source inverter

The DC voltage made constant by the rectifier is delivered by the battery to the inverter input, which thanks to controlled transistor switches, converts this voltage to three-phase AC voltage signal with wide-range variable voltage amplitude and frequency.

The inverter one leg consists of two transistor switches. A simple transistor switch consists of feedback diode connected in antiparallel with transistor.
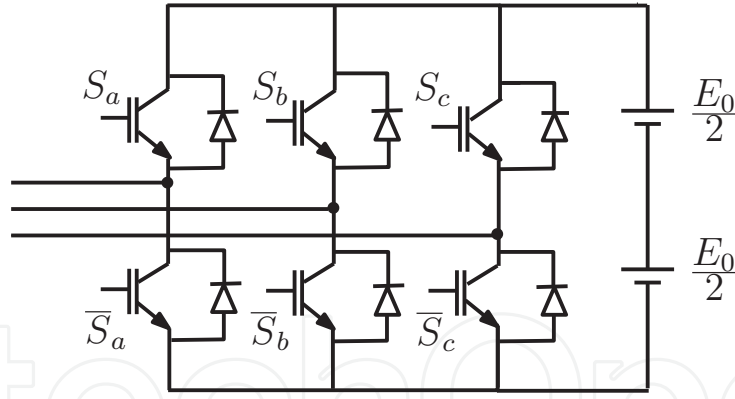
Figure 3.
Two-level three-phase voltage inverter.

Feedback diode conducts current when the load current direction is opposite to the voltage direction.

Assuming that the power devices are ideal, when they are conducting, the voltage across them is zero and they present an open circuit in their blocking mode. Therefore, each inverter leg can be represented as an ideal switch. It gives the possibility to connect each of the three motor phase coils to a positive or negative voltage of the DC link (E_0).

Considering a two-level inverter, presented by **Figure 3**, the voltage vector of the three-phase voltage inverter is represented as follows:

$$\vec{V_s} = \sqrt{\frac{2}{3}} \left[S_a + S_b e^{j\frac{2\pi}{3}} + S_c e^{j\frac{4\pi}{3}} \right] \tag{2}$$

where S_a, S_b, and S_c are three-phase inverter switching functions, which can take a logical value of either 0 or 1.

3. Mathematical model of PMSM in (a, b, c) frame

An accurate dynamic model of the PMSM is necessary to study the dynamic behavior of the machine. Indeed, the dynamic behavior of a PMSM is described in terms of space variables as follows:

$$V_{abc} = R_s I_{abc} + L_s \frac{d}{dt} I_{abc} + \frac{d}{dt} \Phi_{mabc} \tag{3}$$

considering $V_{abc} = [v_a \ v_b \ v_c]^T$, $I_{abc} = [i_a \ i_b \ i_c]^T$, and

$$\frac{d\Phi_{mabc}}{dt} = \Phi_m \omega_r \left[\cos(\theta_r) \ \cos\left(\theta_r - \frac{2\pi}{3}\right) \ \cos\left(\theta_r + \frac{2\pi}{3}\right) \right]^T$$

where V_{abc}, I_{abc}, and Φ_m denote the stator voltages, the stator currents, and the permanent magnetic flux amplitude, respectively. R_s and L_s denote the stator resistance and inductance matrix, respectively.

$$\Phi_{mabc} = \Phi_m \begin{bmatrix} \sin(\theta_r) \\ \sin\left(\theta_r - \frac{2\pi}{3}\right) \\ \sin\left(\theta_r + \frac{2\pi}{3}\right) \end{bmatrix} \tag{4}$$

since $\omega_r = N_p\omega_m$, ω_r and ω_m torque pulsation and mechanical pulsation, respectively. θ_r is the angular position of the rotor with respect to the magnetic axis of the phase (a) of the stator, $\theta_r = N_p\theta_m$, θ_m denotes the mechanical angular position of the rotor, and N_p is the pole pair number.

The electromagnetic torque can be expressed as follows:

$$T_{em} = \frac{e_a i_a + e_b i_b + e_c i_c}{\Omega_m} \tag{5}$$

where e_a, e_b, and e_c are the emf of the phases a, b, and c and $\Phi_{mabcf} = \Phi_m[e_a\ e_b\ e_c]$. Then referring to Eq. (4), the developed equation of electromagnetic torque becomes

$$T_{em} = \frac{\Phi_m\left(\sin(\theta_r)i_a + \sin\left(\theta_r - \frac{2\pi}{3}\right)i_b + \sin\left(\theta_r + \frac{2\pi}{3}\right)i_c\right)}{\Omega_m} \tag{6}$$

The mechanical part of the machine is described by

$$J\frac{d}{dt}\Omega_m = T_{em} - T_l \tag{7}$$

where J is the motor inertia, T_{em} is the electromagnetic torque, and T_l is the load torque.

4. Modeling of the PMSM with inter-turn fault

An inter-turn fault represents an insulation failure between two windings in the same phase of the stator [23].

The representation of a PMSM with stator winding turn fault at phase (a) is shown in **Figure 4**; a_2 and a_1 represent the shorted turns and the healthy turns, respectively. The fault is modeled by a small resistance R_f connected across the shorted turns. In fact, R_s denotes the inter-turn short circuit resistance.

To represent the impact of the defect, a new parameter σ is introduced. Parameter σ is defined as the ratio between the number of shorted turns N_{cc} and the total number of turns N_s.

The resistances of the sub-winding a_1 and the shorted sub-winding a_2 are noted by R_{a1} and R_{a2}, respectively; they are proportional to the number of turns of the involved parties. Therefore, we can express them according to the resistance R_a and the coefficient σ. So we have

$$R_{a_1} = (1 - \sigma)R_a, \quad R_{a_2} = \sigma R_a \tag{8}$$

By defining the electrical quantities of the new circuit with the index "f", and refering to **Figure 5** the new equations of the motor voltages are reformulated as follows:

$$
\begin{aligned}
V_a = &(R_{a_1} + R_{a_2})i_a + (L_{a_1} + L_{a_2} + 2M_{a_1a_2})\frac{di_a}{dt} + (M_{a_1b} + M_{a_2b})\frac{di_b}{dt} \\
&+ (M_{a_1c} + M_{a_2c})\frac{di_c}{dt} + (e_a + e_f) - R_{a_2}i_f - (L_{a_2} + M_{a_1a_2})\frac{di_f}{dt} \\
V_b = &R_s i_b + L\frac{di_b}{dt} + (M_{a_1b} + M_{a_2b})\frac{di_a}{dt} + M\frac{di_c}{dt} + e_b - M_{a_2b}\frac{di_f}{dt} \\
V_c = &R_s i_c + L\frac{di_c}{dt} + (M_{a_1c} + M_{a_2c})\frac{di_a}{dt} + M\frac{di_b}{dt} + e_c - M_{a_2c}\frac{di_f}{dt}
\end{aligned} \tag{9}
$$
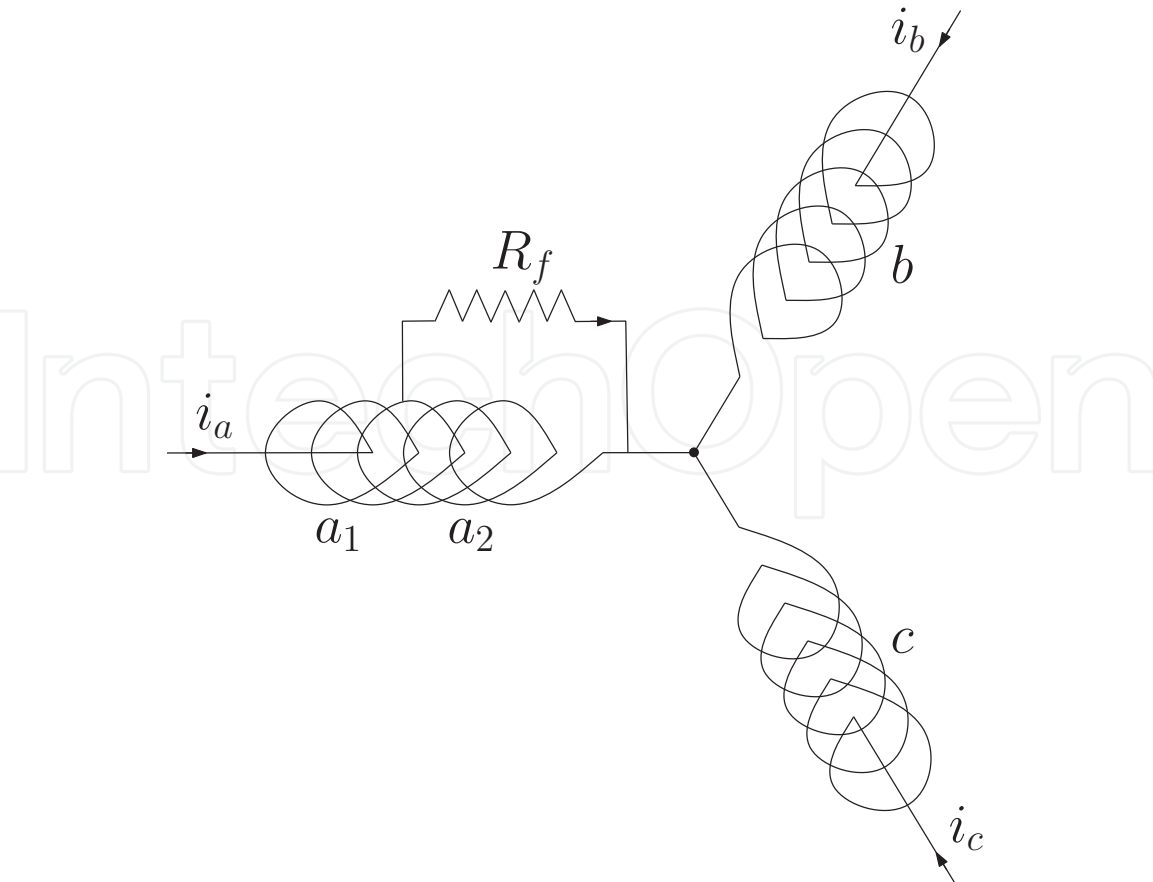
Figure 4.
Equivalent circuit of PMSM under inter-turn fault in phase (a).
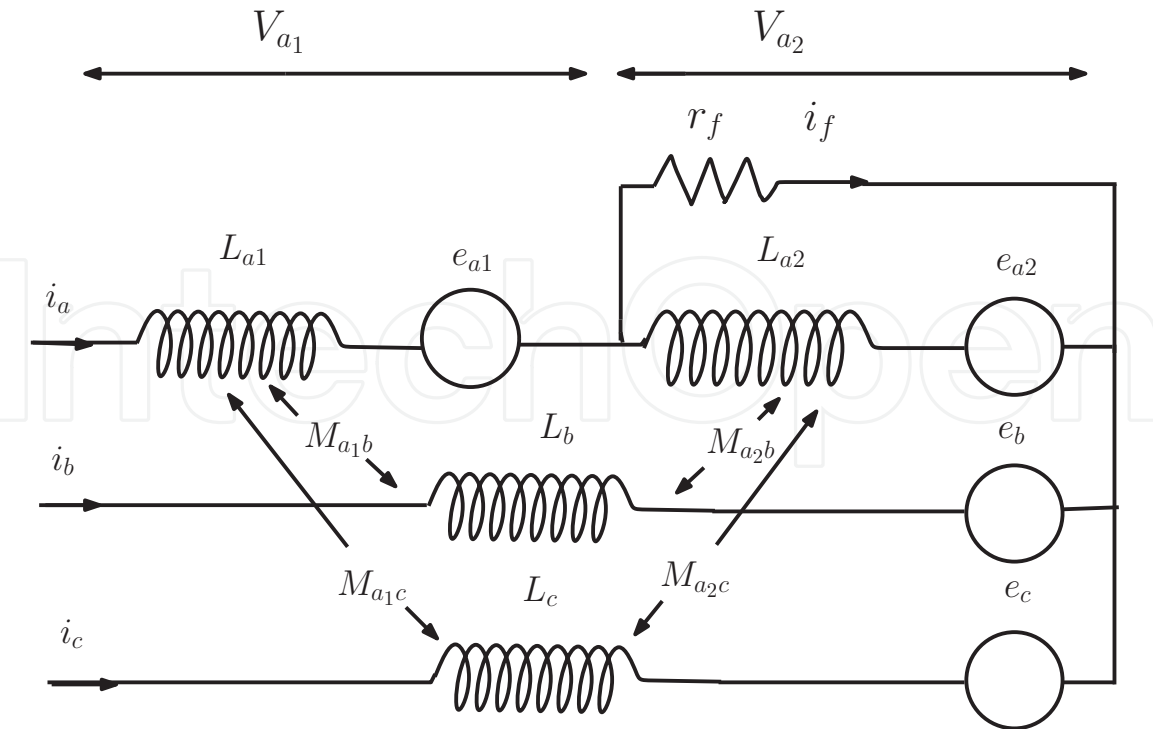
Figure 5.
Schematic representation of an insulation fault between turns on a phase of the stator.

where L and M denote the phase self-inductance and M is the mutual inductance between phase windings of healthy PMSM, respectively. And considering $L_{a_1} = (1 - \sigma)^2 L_a$, $L_{a_2} = \sigma^2 L_a$ and $M_{a_1 a_2} = \sigma(1 - \sigma)L_a$.

5. Design of a conventional DTC-SVM traction system

The disadvantages of basic DTC is obvious: torque and flux ripples, deteriorated performance at low speed, and uncontrolled switching frequency of the inverter. For the defects of basic DTC, much works have been made over the past few decades. DTC combined with space vector modulation (DTC-SVM) for PMSM is to accomplish constant switching frequency of the inverter in addition to obtain the desired torque and stator flux with little ripples by synthesizing an appropriate voltage space vector through SVM, which is more accurate than that of basic DTC to compensate the error of desired and actual stator flux.

5.1 Flux reference coordinate computing

The relationship between the voltage, current, and stator flux vectors of a PMSM is given by

$$\frac{d}{dt}\overline{\Phi}_s = \overline{V}_s - R_s\overline{I}_s \tag{10}$$

where R_s is the stator resistance.

The reference of stator flux amplitude and phase is stated using *Concordia* quantities as

$$|\Phi_s^*| = \sqrt{\phi_{\alpha s}^{*2} + \phi_{\beta s}^{*2}}, \quad \theta_s^* = \arctan\left(\frac{\phi_{\beta s}^*}{\phi_{\alpha s}^*}\right) \tag{11}$$

5.2 Voltage reference coordinate computing

The coordinates of references of voltage vectors $v_{\alpha s}^*$ and $v_{\beta s}^*$ in (α, β) frame are determined by the following equations:

$$\begin{cases} v_{\alpha s}^* = \dfrac{\phi_{\alpha s}^* - \phi_{\alpha s}}{T_{em}} + R_s i_{\alpha s} \\[2mm] v_{\beta s}^* = \dfrac{\phi_{\beta s}^* - \phi_{\beta s}}{T_{em}} + R_s i_{\beta s} \end{cases} \tag{12}$$

These vectors are introduced to the SVM block, which use them to control the inverter switches (S_a, S_b, S_c).

5.3 SVM block design

The SVM technique refers to a special switching scheme of the six power transistors of a two-level three-phase voltage inverter. In fact, it uses eight sorts of different switch modes of the inverter to control the stator flux to advance the reference flux circle. Eight types of switch modes stand for eight space voltage vectors that contain six active voltage vectors and two zero voltage vectors as shown in **Figure 6a** [30, 31].

Voltage vectors, created by a three-phase PWM inverter, divide the space vector plane into six sectors: $(i-1)\frac{\pi}{3} < S_i \leq i\frac{\pi}{3}, i = 1, ..., 6$. The determination of the sector, where the reference voltage vector is located, is done according to
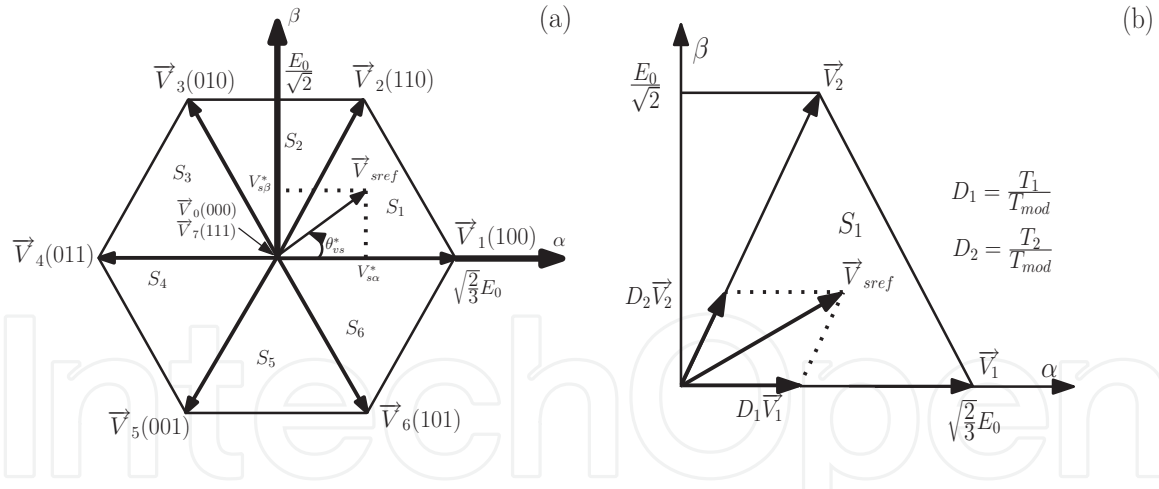
Figure 6.
(a) Basic switching vectors and sectors. (b) Projection of the reference voltage vector on two adjacent vectors.

$$\theta_s^* = \arctan\left(\frac{v_{\beta s}^*}{v_{\alpha s}^*}\right) \tag{13}$$

The SVM's principle is to project the desired stator voltage vector $\vec{V}_{sref}$ on the two adjacent voltage vectors $\vec{V}_i$ and $\vec{V}_{i+1}$ corresponding to two switching states of the inverter. Values of these projections provide the determination of desired commutation times T_i and T_{i+1} and correspond to two nonzero switching states of the inverter. To maintain the constant commutation frequency, in the case where $T_i + T_{i+1} \leq T_{mod}$, a zero state of the inverter is applied during the rest of the period T_{mod}, i.e., $T_0 = T_{mod} - (T_i + T_{i+1})$. In what follows, the study will be limited to sector S_1, as presented in **Figure 6b**. As the reference voltage vector $\vec{V}_{sref}$ is in sector S_1, it can be compounded by the active voltage vectors V_1 and V_2. The projection on these adjacent vectors gives the following expression:

$$
\begin{aligned}
\vec{V}{sref} &= V_{s\alpha}^* + jV_{s\beta}^* \\
&= \frac{T_1}{T_{mod}}\vec{V}_1 + \frac{T_2}{T_{mod}}\vec{V}_2
\end{aligned}
\tag{14}
$$

where $T_{mod} = T_1 + T_2 + T_0$. D_1 and D_2 are duties relative to voltages V_1 and V_2. In sector S_1, expressions of the voltage vectors are

$$
\begin{cases}
\vec{V}_1 = \sqrt{\frac{2}{3}}E_0(\cos 0 + j\sin 0) = \sqrt{\frac{2}{3}}E_0 \\
\vec{V}_2 = \sqrt{\frac{2}{3}}E_0\left(\cos\frac{\pi}{3} + j\sin\frac{\pi}{3}\right)
\end{cases}
\tag{15}
$$

Expressions of T_1 and T_2 are detailed in the sequel:

$$
\begin{cases}
T_1 = \left(\sqrt{\frac{3}{2}}V_{s\alpha}^* - \frac{1}{\sqrt{2}}V_{s\beta}^*\right)\frac{T_{mod}}{E_0} \\
T_2 = \sqrt{2}V_{s\beta}^*\frac{T_{mod}}{E_0}
\end{cases}
\tag{16}
$$

Consequently, the expressions of the duties are given as follows:

$$
\begin{cases}
D_1 = \left(\sqrt{\dfrac{3}{2}} V_{s\alpha}^* - \dfrac{1}{\sqrt{2}} V_{s\beta}^* \right) \dfrac{1}{E_0} \\[3mm]
D_2 = \sqrt{2} V_{s\beta}^* \dfrac{1}{E_0}
\end{cases}
\tag{17}
$$

The time duration of each nonzero vector is divided equally into two parts, the time duration of zero vectors is distributed equally to $\vec{V}_0$ and $\vec{V}_7$, and thus the switching sequence of space vector is $\vec{V}_0, \vec{V}_1, \vec{V}_2, \vec{V}_7, \vec{V}_7, \vec{V}_2, \vec{V}_1, \vec{V}_0$ during the modulation period.

The duties of each phase of the inverter are calculated as follows:

$$
\begin{cases}
D_a = D_1 + D_2 + \dfrac{1}{2} D_0 \\[3mm]
D_b = D_2 + \dfrac{1}{2} D_0 \\[3mm]
D_c = \dfrac{1}{2} D_0
\end{cases}
\tag{18}
$$

As $D_1 + D_2 + D_0 = 1$, duties, given by the system of Eq. (18), turn to be

$$
\begin{cases}
D_a = \dfrac{1}{2} \left(1 + \sqrt{\dfrac{3}{2}} \dfrac{V_{s\alpha}^*}{E_0} + \dfrac{1}{\sqrt{2}} \dfrac{V_{s\beta}^*}{E_0} \right) \\[3mm]
D_b = \dfrac{1}{2} \left(1 - \sqrt{\dfrac{3}{2}} \dfrac{V_{s\alpha}^*}{E_0} + \dfrac{1}{\sqrt{2}} \dfrac{V_{s\beta}^*}{E_0} \right) \\[3mm]
D_c = \dfrac{1}{2} \left(1 - \sqrt{\dfrac{3}{2}} \dfrac{V_{s\alpha}^*}{E_0} - \dfrac{1}{\sqrt{2}} \dfrac{V_{s\beta}^*}{E_0} \right)
\end{cases}
\tag{19}
$$

5.4 Block diagram of the DTC-SVM

The DTC-SVM block diagram retains all the advantages of the conventional DTC, such as no coordinate transformation, robust to motor parameters, etc. Moreover, a SVM block is used to generate the pulses for the inverter in order to promise a fixed commutation frequency.

Figure 7 illustrates the block diagram of the proposed traction control system, and the overall control scheme is set as follows:

- Including two major loops: the torque control loop and the flux control loop. In fact, the flux and torque are directly controlled individually. The basic principle of the direct torque control is to destine the torque error and the flux error in hysteresis bands by properly choosing the switching states of the inverter.

- The speed command is compared with the estimating speed to compute the speed error. Then, the speed error is processed by the PI speed controller to obtain the torque command. On the other hand, the flux command is compared to the estimated flux.

- The errors ΔT_{em} and $\Delta \Phi_s$ go through the hysteresis controllers and the vector selection table to generate the required switching states and therefore the desired voltage vector.
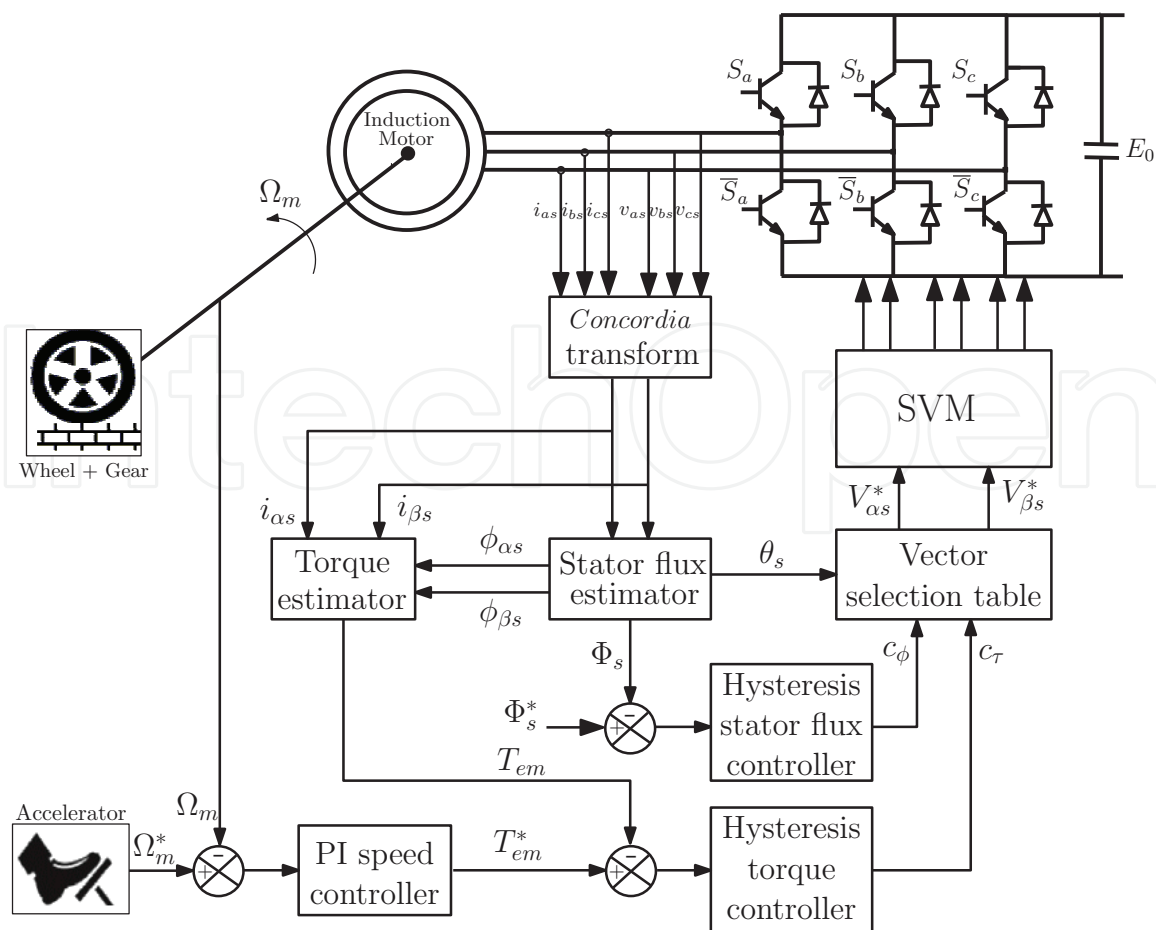
Figure 7.
Block diagram of SVM-DTC PMSM drive.

- The controllers produce the voltage command vector; an appropriate space voltage vector can be generated with SVM.

6. Simulation end discussion

Parameters of the PMSM are listed in **Table 1**. It has the following ratings: 220 V, 10 kW, and 1470 rpm at 50 Hz.

The parameters of the electric vehicle model are given in **Table 2**.

6.1 Case study

We consider a vehicle traveling along a straight horizontal road. For $F_{hc} = 0$, the tractive effort is reduced to $F_{te} = F_{rrol} + F_{ad}$, and the load torque can be expressed as $T_r = R_g r(F_{rrol} + F_{ad}) =$, where $R_g = \frac{1}{G}$ and G denotes the gear ratio.

After development the load torque is

$$T_l \;=\; K_1 + K_2 V_v^2 \tag{20}$$

$R_s = 0.29\Omega$	$L_s = L_r = 50$ mH	$N_p = 2$
$R_r = 0.38\Omega$	$M = 47.3$ mH	$J = 0.5$ Kg.m^2

Table 1.
PMSM parameters.

$r = 0.3m$	$A = 1m^2$
$M_v = 400$ Kg	$C_d = 0.19$
$G = 0.9$	$\rho = 1.2$ Kg/m^3

Table 2.
The electric vehicle model parameters.

where $K_1 = R_g r \mu M_v g$ and $K_2 = \frac{1}{2} R_g r \rho A C_d V_v^2$.
The relationship between vehicle speed and motor speed is given by

$$V_v = R_g r \ \Omega_m \tag{21}$$

Simulation tests were performed in healthy and faulty conditions, with the motor driving a load torque, referring to Eqs. (20) and (21), and can be expressed as follows:

$$T_l \ = \ K_1 + K_2 (R_g r)^2 \Omega_m^2 \tag{22}$$

The magnitude of the torque and flux hysteresis bands is 0.01 N.m and 0.001 Wb, respectively.

6.2 Steady-state operation analysis

Figure 8 shows several features of the PMSM drive at steady-state operation considering a speed $\Omega_m = 750$ rpm. Waveforms presented in the left side (subscript "1") of **Figure 8** represent results yielded by the PMSM under DTC-SVM without fault. The middle side (subscript "2") of **Figure 8** represents the results yielded by the PMSM under DTC-SVM considering 5% turns are shorted. The right side
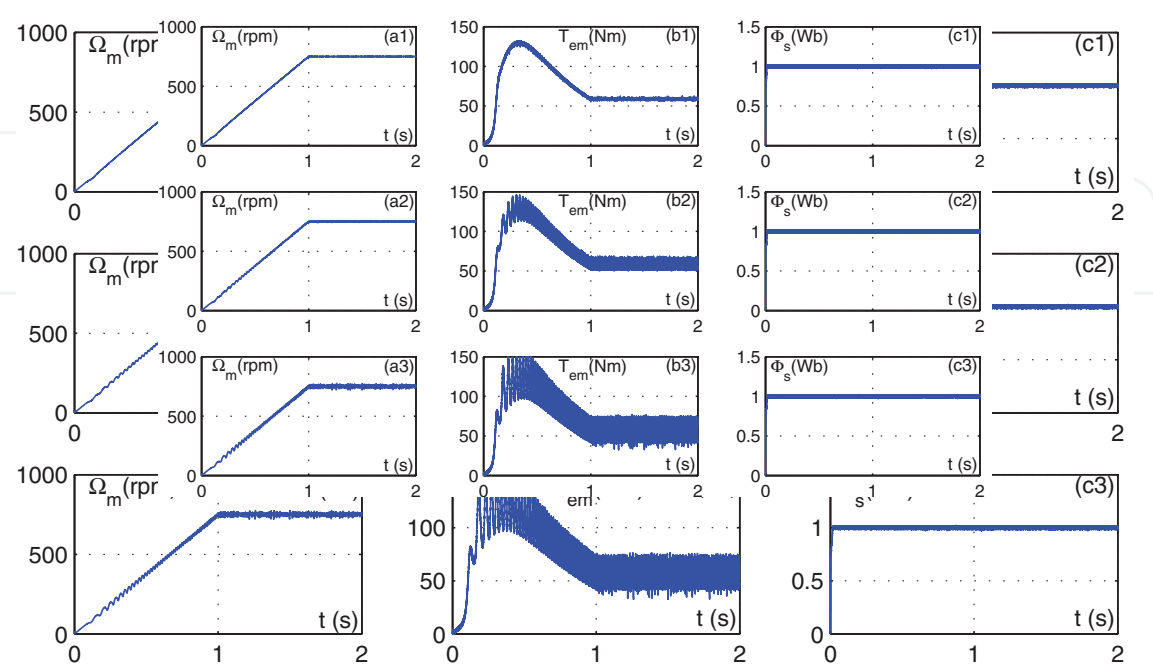
Figure 8.
(subscript "1") Considering the PMSM under DTC-SVM without fault, (subscript "2") considering the PMSM under DTC-SVM allowing for 5% shorted turns, and (subscript "3") considering the PMSM under DTC-SVM allowing for 25% shorted turns. Legend: (a) speed and its reference, (b) electromagnetic torque, and (c) stator phase current.

(subscript "3") of **Figure 8** represents the results yielded by PMSM under DTC-SVM considering 25% turns are shorted.

From the analysis of the previous steady-state simulation results, one can remark the following:

- The speed follows its reference despite the presence of defect. It is clear that in the case of machine with short circuit fault, the speed oscillates around its reference with a ripple amplitude that increases when the percentage of turns shorted increases.

- It is seen in **Figure 8** when 5 and 25% turns are shorted, respectively, in one of the phase (a) windings, the increase of torque ripples is notable.

- The stator flux shapes, in healthy and faulty conditions, are quite similar.

6.3 Signature extraction based on the analysis of the fault effect

From the analysis of **Figure 9**, one can notice that a short circuit fault between turns on phase (a) increases the amplitude of the second harmonic which was too low in the spectrum of the healthy machine. This harmonic introduced by the defect presents an amplitude that evolves the rate of defect in the sense that this harmonic sees its amplitude increases in a proportional way with the increase of the number of turns short circuited on the phase (a). When we increase the rate of the short circuit, the amplitude of this harmonic has increased in value.
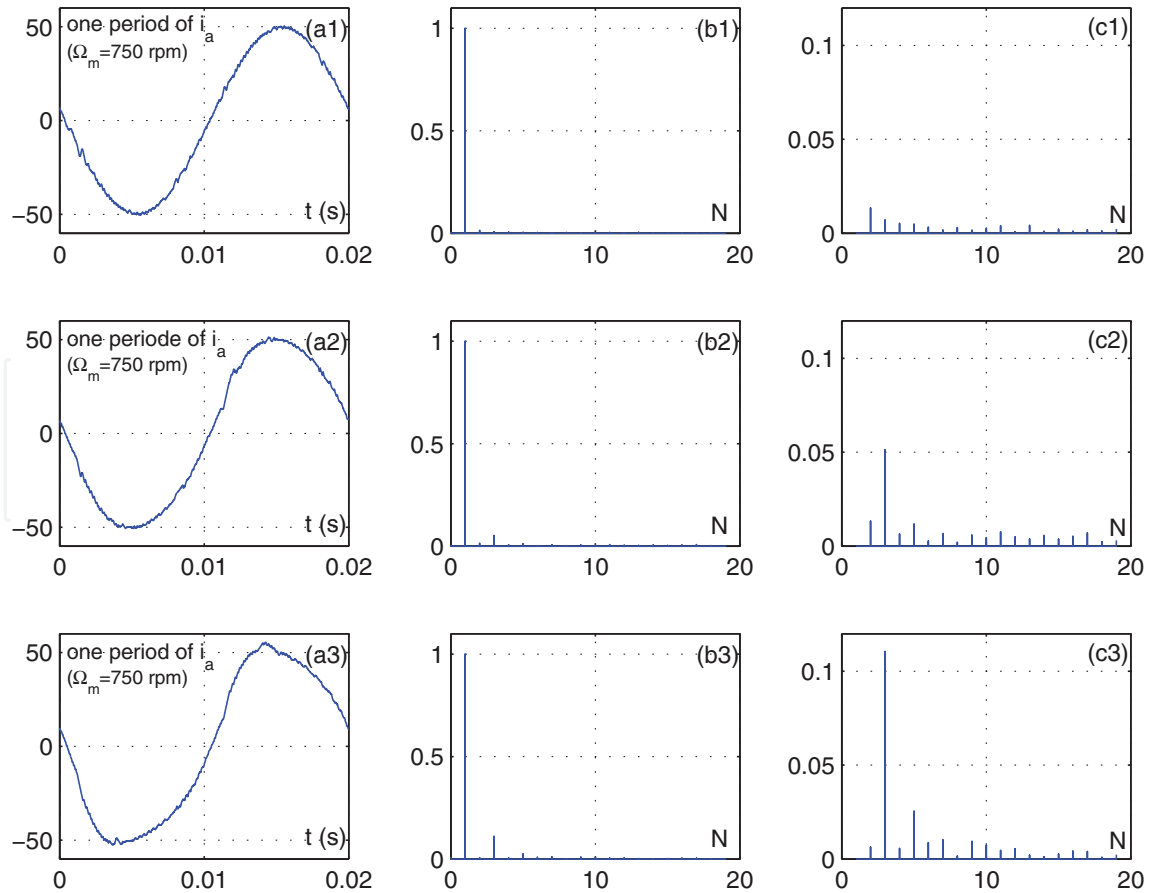
Figure 9.
(a) One period of i_{as}, (b) reduced spectrum of i_{as} with respect to fundamental, and (c) harmonic of i_{as} (fundamental = 1). (subscript "1") considering the PMSM under DTC-SVM without fault, (subscript "2") considering the PMSM under DTC-SVM allowing for 5% shorted turns, and (subscript "3") considering the PMSM under DTC-SVM allowing for 25% shorted turns.

In light of this analysis, it clearly appears that, in general, the harmonic amplitude increases in an apparent way when there is a short circuit fault.

7. Conclusion

The chapter focused on a study and diagnosis of the PMSM under DTC-SVM integrated in EV propulsion system without and with stator winding fault. Simulation results have been presented in order to demonstrate that in a DTC-SVM PMSM drive, with stator inter-turn short circuits, the considered defect affects the dynamics of the motor and introduces a strong second harmonic in the motor supply currents, which can be used to detect this type of fault. This ascertainment can be used in the industry for fault detection and diagnosis of stator winding faults of PMSM.

Author details

Fatma Ben Salem
Control and Energy Management Laboratory (CEMLab), University of Sfax, Sfax Engineering School, Sfax, Tunisia

*Address all correspondence to: fatma.bensalem@isgis.usf.tn; fatma_bs@yahoo.fr

References

[1] Erdogan S, Miller-Hooks E. A green vehicle routing problem. Transportation Research Part E: Logistics and Transportation Review. 2012;**48**(1): 100-114

[2] Serra JVF. Electric Vehicles Technology, Policy and Commercial Development. London, UK: Earthscan; 2013

[3] Felipe A, Ortuno MT, Righini G, Tirado G. A heuristic approach for the green vehicle routing problem with multiple technologies and partial recharges. Transportation Research Part E: Logistics and Transportation Review. 2014;**71**(1):111-128

[4] Longo M, Foiadelli F, Yaïci W. Electric vehicles integrated with renewable energy sources for sustainable mobility. In: New Trends in Electrical Vehicle Powertrains. IntechOpen; 2018

[5] Habetler TG, Profumo F, Pastorelli M, Tolbert LM. Direct torque control of induction machines using space vector modulation. IEEE Transactions on Industry Applications. 1996;**28**(5):1045-1053

[6] Bounadja M, Belarbi A, Belmadani B. A high performance space vector modulation—Direct torque controlled induction machine drive based on stator flux orientation technique. Advances in Electrical and Computer Engineering. 2009;**9**(2):28-33

[7] Joseline Metilda A, Arunadevi R, Ramesh N, Sharmeela C. Analysis of direct torque control using space vector modulation for three phase induction motor. Recent Research in Science and Technology. 2011;**3**(7):37-40

[8] Nasri A, Gasbaoui B. A novel electric vehicle drive studies based on space vector modulation technique and direct torque. Journal of Asian Electric Vehicles. 2011;**9**(2):1529-1535

[9] Rashag HF, Koh SP, Chong KH, Tiong SK, Tan NML, Abdalla AN. High performance of space vector modulation direct torque control SVM-DTC based on amplitude voltage and stator flux angle. Research Journal of Applied Sciences, Engineering and Technology. 2013;**5**(15):3934-3940

[10] Ahammad N, Khan SA, Reddy RK. Novel DTC-SVM for an adjustable speed Sensorless induction motor drive. International Journal of Science Engineering and Advance Technology (IJSEAT). 2014;**2**(1):31-36

[11] Rashag HF, Tan NML, Koh SP, Abdalla AN, Chong KH, Tiong SK. DTC-SVM based on PI torque and PI flux controllers to achieve high performance of induction motor. Research Journal of Applied Sciences, Engineering and Technology. 2014;**7**(4):875-891

[12] Ben Salem F, Derbel N. Second-order sliding-mode control approaches to improve low-speed operation of induction machine under direct torque control. International Journal of Electric Power Components and Systems. 2016; **44**(17):1969-1980

[13] Ben Salem F, Yangui A, Masmoudi A. On the reduction of the commutation frequency in dtc: A comparative study. European Transactions on Electrical Power Engineering. 2005;**15**(6):571-584

[14] Chlebis P, Brandstetter P, Palacky P. Direct torque control of induction motor with direct calculation of voltage vector. Advances in Electrical and Computer Engineering. 2010;**4**:17-22

[15] Chaikhy H, Khafallah M, Saad A. Evaluation of two control strategies for induction machine. International Journal of Computers and Applications. 2011;**35**(5):571-584

[16] Allirani S, Jagannathan V. Direct torque control technique in induction motor drives—A review. Journal of Theoretical and Applied Information Technology. 2014;**60**(3):454-475

[17] Qi H, Li J, Chen Y. Control of electric vehicle. In: Soylu S, editor. Urban Transport and Hybrid Vehicles. IntechOpen; 2010. p. 192. ISBN 978-953-307-100-8

[18] Gieras JF, Wing M. Permanent Magnet Motor Technology, Design and Application. Electrical and Computer Engineering. 3rd edition. Boca Raton, London, New York: CRC Press Taylor and Francis Group; 26 August 2009

[19] Singh R, Sengar KP, Mishra A, Thakur C. A direct torque control of interior permanent magnet synchronous motor for an electric vehicle-design analysis total harmonic distortion of stator current. International Journal of Engineering Research & Technology (IJERT). 2016;**5**(11):57-65

[20] Hadef M, Mekideche MR, Djerdir A. Vector controlled permanent magnet synchronous motor (PMSM) drive with stator turn fault. In: Proceeding of XIX International Conference; Rome: ICEM; 6-8 September 2010

[21] Jeong Y, Sul S, Schulz SE, Patel NR. Fault detection and fault-tolerant control of interior permanent-magnet motor drive system for electric vehicle. IEEE Transactions on Industry Applications. 2005;**41**(1):46-51

[22] Ebrahimi B-M, Faiz J. Feature extraction for short-circuit fault detection in permanent-magnet synchronous motors using stator-current monitoring. IEEE Transactions on Power Electronics. 2010;**25**(10): 2673-2682

[23] Hadef M, Djerdir A, Mekideche MR, N'Diaye AO. Diagnosis of stator winding short circuit faults in a direct torque controlled interior permanent magnet synchronous motor. In: IEEE Vehicle Power and Propulsion Conference; Chicago, IL, USA; 6-9 September 2011; DOI: 10.1109/VPPC.2011.6043166

[24] Haddad RZ, Strangas EG. Fault detection and classification in permanent magnet synchronous machines using fast Fourier transform and linear discriminant analysis. 2013. pp. 99-104

[25] Kamdi PD, Vaidya UB, Kamdi SY, Asutakar P. Diagnosis of stator winding short circuit fault in permanent magnet synchronous motor. International Research Journal of Engineering and Technology (IRJET). 2015;**2**(4):325-328

[26] Rohan A, Rabah M, Kim SH. An integrated fault detection and identification system for permanent magnet synchronous motor in electric vehicles. International Journal of Fuzzy Logic and Intelligent Systems. 2018; **18**(1):20-28. DOI: 10.5391/IJFIS.2018.18.1.20

[27] Liang H, Chen Y, Liang S, Wang C. Fault detection of stator inter-turn short-circuit in PMSM on stator current and vibration signal. Applied Sciences. 2018;**8**:1677. DOI: 10.3390/app8091677

[28] Larminie J, Lowry J. Electric Vehicle Technology Explained. 2nd ed. Vol. 23. Chichester, England: John Wiley & Sons, Ltd; 2012

[29] Wang Z, Qu C, Zhang L, Zhang J, Yu W. Integrated sizing and energy management for four-wheel-independently-actuated electric vehicles considering realistic constructed driving cycles. Energies. 2018;**11**:1768. DOI: 10.3390/en11071768.

[30] Ben Salem F, Derbel N. VSC-based DTC-SVM with adaptive parameter estimation. In: IEEE 11th Int. Conf. on Systems, Signals and Devices (SSD'14),

Castelldefels-Barcelona; 11-14 February 2014; Spain

[31] Ben Salem F, Derbel N. Direct torque control of induction motors based on discrete space vector modulation using adaptive sliding mode control. International Journal of Electric Power Components and Systems. 2014; **42**(14):1598-1610